PNAS RESEARCH ARTICLE | IMMUNOLOGY AND INFLAMMATION

Dissection of complement and Fc-receptor-mediated pathomechanisms of autoantibodies to myelin oligodendrocyte glycoprotein

Simone Mader[a], Samantha Ho[a,b,1], Hoi Kiu Wong[a,1], Selia Baier[a,1], Stephan Winklmeier[a], Carolina Riemer[c], Heike Rübsamen[a], Iris Marti Fernandez[a], Ramona Gerhards[a], Cuilian Du[a], Omar Chuquisana[d], Jan D. Lünemann[d], Anja Lux[c], Falk Nimmerjahn[c,e], Monika Bradl[f,2], Naoto Kawakami[a,2], and Edgar Meinl[a,2,3]

Edited by Lawrence Steinman, Stanford University, Stanford, CA; received January 18, 2023; accepted February 8, 2023

Autoantibodies against myelin oligodendrocyte glycoprotein (MOG) have recently been established to define a new disease entity, MOG-antibody-associated disease (MOGAD), which is clinically overlapping with multiple sclerosis. MOG-specific antibodies (Abs) from patients are pathogenic, but the precise effector mechanisms are currently still unknown and no therapy is approved for MOGAD. Here, we determined the contributions of complement and Fc-receptor (FcR)-mediated effects in the pathogenicity of MOG-Abs. Starting from a recombinant anti-MOG (mAb) with human IgG1 Fc, we established MOG-specific mutant mAbs with differential FcR and C1q binding. We then applied selected mutants of this MOG-mAb in two animal models of experimental autoimmune encephalomyelitis. First, we found MOG-mAb-induced demyelination was mediated by both complement and FcRs about equally. Second, we found that MOG-Abs enhanced activation of cognate MOG-specific T cells in the central nervous system (CNS), which was dependent on FcR-, but not C1q-binding. The identification of complement-dependent and -independent pathomechanisms of MOG-Abs has implications for therapeutic strategies in MOGAD.

Autoimmunity | neuroimmunology | inflammation | demyelination | effector mechanisms

Significance

Autoantibodies against myelin oligodendrocyte glycoprotein (MOG) define a new disease, MOG-antibody-associated disease (MOGAD). MOG-Abs from patients are pathogenic, but precise effector mechanisms are unclear and there is no approved therapy. Starting from a pathogenic MOG-specific mAb with a human IgG1 Fc part, we generated mutants with differential FcR and complement binding and studied their pathogenic activity in two animal models. First, MOG-Abs induced demyelination, about equally by FcR activation and complement activation. Second, MOG-Abs enhanced infiltration and activation of cognate T cells via FcRs. Thus a complement-directed therapy, which is effective in neuromyelitis optica spectrum disorders (NMOSD), a related disease with Abs to astrocytes, might not be sufficient in MOGAD. Instead, an FcR-targeted therapy might be more promising in MOGAD.

The identification of autoantibodies allows to stratify patients with inflammatory diseases of the central nervous system (CNS) (1, 2). Some autoantibodies against extracellular targets have been identified to be pathogenic and detailed insights into the different pathomechanisms of CNS-specific autoantibodies were obtained (3, 4). Based on this, therapeutic strategies were successfully applied (4–8). Autoantibodies against myelin oligodendrocyte glycoprotein (MOG) and the astrocyte water channel protein aquaporin-4 (AQP4) define the diseases MOGAD and neuromyelitis optica spectrum disorders (NMOSDs), respectively, which can thereby be distinguished from multiple sclerosis (MS) (9–12). Autoantibodies against AQP4 are potent complement activators (13, 14) and mediate tissue destruction mostly by activation of the terminal complement complex (15, 16); although antibody-mediated cellular cytotoxicity has also been observed for anti-AQP4 Abs (17). This resulted in the therapeutic approach to target the complement component C5 in NMOSD, which greatly reduced relapses in patients (6, 18). Although both MOGAD and NMOSD are inflammatory and demyelinating diseases of the CNS, evidence is increasing that there are different pathomechanisms involved (4). Elucidating the MOG IgG effector mechanisms is highly important as in contrast to NMOSD, no therapy has been approved for MOGAD.

Although the deposition of the complement attack complex C9neo has been observed in brain lesions of MOGAD patients (19–21), it appears less prominent compared to reported histopathological cases of AQP4-IgG-positive NMOSD (16). This suggests that complement inhibition might be less beneficial for MOGAD patients. In vitro studies provided evidence for MOG antibody-mediated pathogenicity in oligodendrocytes (22) and MOG-transfected cells through antibody-dependent cellular cytotoxicity (23). Although MOG-Abs from some high-titer MOGAD patients induce complement-dependent lysis of transfected cells (24) and in myelinating slice cultures (25), a recent study suggested that complement activation by MOG-Abs from MOGAD patients is less efficient than by anti-AQP4-Abs from NMOSD patients (26).

In vivo pathogenicity of MOG-IgG was suggested by transfer experiments (27–31) and confirmed by using affinity-purified MOG-IgG from patients (32). These transfer experiments revealed that MOG-IgG mediates pathology by two different mechanisms. First, MOG-Abs mediate demyelination when the blood–brain barrier (BBB) is breached by T cells as observed in cotransfer experiments with T cells specific for different CNS

The authors declare no competing interest.

This article is a PNAS Direct Submission.

[1]S.H., H.K.W., and S.B. contributed equally to this work.

[2]M.B., N.K., and E.M. contributed equally to this work.

[3]To whom correspondence may be addressed. Email: Edgar.Meinl@med.uni-muenchen.de.

This article contains supporting information online at https://www.pnas.org/lookup/suppl/doi:10.1073/pnas.2300648120/-/DCSupplemental.

Published March 21, 2023.

proteins, including myelin basic protein (MBP) (31, 33), transiently expressed axonal glycoprotein 1 (34), or oligodendrocyte myelin glycoprotein (35). Second, MOG-Abs from patients enhance inflammation of cognate MOG-specific T cells (32), which is mechanistically not understood in detail (28, 29).

Although MOG-IgG has been used in several animal models and MOGAD is now recognized as a distinct disease entity (9, 10), the precise linkage between IgG-Fc effector functions and MOG-IgG-induced pathology remains unclear. Here, we set out to dissect complement and FcR-mediated effects of MOG-IgG. Since MOG-IgG from patients with MOGAD is typically IgG1 (36), this study investigates a monoclonal antibody (mAb) to MOG with a human IgG1 Fc part (r8-18C5) that showed a similar pathogenic activity as affinity-purified MOG antibodies (Abs) from patients in a rodent transfer model (32). Human IgGs activate murine effector cells through all classes of Fcγ receptors (FcγR) (37, 38) and activate the classical complement pathway in rodents (15).

We have generated 13 Fc-mutated variants of the MOG-specific mAb r8-18C5 which have a human IgG1 Fc part and performed a detailed characterization of their binding to C1q and individual Fcγ receptors (FcγR). We then selected variants of the antibodies to dissect FcγR and complement-mediated pathology in vivo, similarly as previously performed for AQP4-IgG (17). We used two different experimental autoimmune encephalomyelitis (EAE) animal models: First, MOG-Abs were injected following MBP-specific T cells, which strongly breach the blood–brain barrier (BBB), and demyelination was quantified histologically. Second, MOG-Abs were applied together with EGFP-labeled MOG-specific T cells to quantify the effects of MOG-IgG variants on the infiltration of cognate MOG-specific T cells and bystander cells. Thereby, we found that MOG-IgG could enhance inflammation and mediate demyelination independent of complement activation, but dependent on Fc-receptor (FcR) engagement. Our findings have important implications for understanding the pathogenic mechanisms of anti-MOG-IgG-directed autoimmunity and for therapeutic strategies in MOGAD.

Results

MOG-Specific mAb Mutants with Differential C1q and FcR Binding. We constructed 13 mutations of the Fc part of our humanized anti-MOG IgG1 mAb r8-18C5 based on prior publications with the aim to differentially affect C1q and FcγR binding (*SI Appendix*, Table S1). As expected, the mutations of the Fc part did not affect MOG recognition (Fig. 1*A* and *SI Appendix*, Fig. S1*A*). We determined the C1q binding of the different mAb mutants by enzyme-linked immunosorbent assay (ELISA) and identified several Fc mutants that lacked C1q binding (Fig. 1*B* and *SI Appendix*, Fig. S1*B*). Next, we also measured their binding to different FcγRs using an immunocomplex ELISA with MOG and recombinant FcγRs (Fig. 1 *C*–*G* and *SI Appendix*, Fig. S1 *C*–*F*). Here, we observed antibodies with either abolished binding to FcγRI and FcγRIV (LL, LLP, TAP, T299L, TKQ) or intact binding to FcγRI and FcγRIV (E345K, E430G, KE, KQ, K322A, AP) (*SI Appendix*, Fig. S1 *C*–*F*). The SAI mutant had intact binding to FcγRI and FcγRIV (Fig. 1 *D* and *G* and *SI Appendix*, Fig. S1 *C* and *F*) as expected (*SI Appendix*, Table S1). While the optical density (OD) values for FcγRI and FcγRIV were measured after 40 min, FcγRIIb and FcγRIII were developed up to 300 min, reflecting low affinity (39).

These mutants allowed us to dissect C1q and FcγR binding of MOG-IgG. Based on this characterization, we selected one Fc-mutant antibody that had abolished C1q binding but maintained FcγR binding (SAI mutant) and one that had lost both C1q binding and showed little or no binding to FcγRI and FcγRIV (TAP mutant) for our further in vivo experiments.

MOG-Abs Mediate Demyelination by Both Complement Activation and FcγR Engagement. To study the pathogenic effect of the selected MOG-Fc mutant Abs, TAP, and SAI, we employed two different EAE models: In our first model, MBP-specific T cells induce a mild EAE (Fig. 2), inflammation demonstrated by $ED1^+$ macrophages/microglia without demyelination, and breach the BBB demonstrated by influx of human IgG (hIgG) (Fig. 3*A*). In this model, the r8-18C5 enhanced clinical disease (Fig. 2) and induced demyelination (Fig. 3 *A* and *B*), which is in accordance with our previous observation (32).

The SAI mutant (lacking C1q binding, but retaining FcγR binding) enhanced the clinical disease similar to the MOG antibody r8-18C5 (Fig. 2). We detected deposition of the injected human IgG in the spinal cord in all animals treated with MBP-specific T cells, which indicates breaching of the BBB (Fig. 3*A*). Our histopathological analysis revealed that the SAI mutant was able to induce demyelination albeit to a lesser degree than the anti-MOG-Ab, r8-18C5 (Fig. 3 *A* and *B*). Our study shows that in the absence of complement activation, about half of the demyelination is observed, which is mediated via FcR activation. Staining for the terminal complement complex C9neo revealed a strong induction by r8-18C5, but not by the SAI mutant (Fig. 3*A*).

In contrast, when the TAP mutant (lacking C1q binding with little or no FcγR binding) was applied, clinical disease was similar as with the isotype control HK3 (Fig. 2). This mutant did not induce demyelination in the inflamed CNS (Fig. 3 *A* and *B*) and there was no C9neo deposition observed despite the detected presence of IgG binding (Fig. 3*A*). Thus, the MOG-specific Ab with the TAP mutant did not enhance disease in this model, neither clinically nor histologically; it was comparable to the control antibody, which does not show binding to the myelin sheath (Fig. 3*A*).

MOG-Abs Enhance Activation and Infiltration of Cognate T Cells via FcγR Engagement. In our second model, treatment with MOG-specific T cells together with the isotype control antibody HK3 did not induce clinical disease (Fig. 4), while a slight inflammation was observed predominantly in the meninges (Fig. 5*A*). In this model, cotreatment of anti-MOG Ab r8-18C5 was associated with clinical disease and enhanced inflammation (Fig. 5 *A* and *B*) as previously reported (32).

The MOG-mAb with the SAI mutant enhanced clinical disease to a similar degree as r8-18C5 (Fig. 4). Histological analysis indicated that the enhanced T cell infiltration was accompanied by increased infiltration of $ED1^+$ macrophages/microglia in animals that were injected with r8-18C5 or SAI (Fig. 5 *A* and *B*). We quantified the number of MOG-specific T cells making use of MOG-GFP-labeled T cells by flow cytometry. This showed that the SAI mutant enhanced infiltration of MOG-specific T cells similarly as the r8-18C5 (Fig. 5*C*). We also evaluated the activation state of the infiltrating MOG-specific T cells and compared this with the bystander T cells by quantifying the activation marker OX40 on MOG-specific GFP-labeled cells by fluorescence activated cell sorting (FACS). This showed that both the SAI mutant and the anti-MOG Ab r8-18C5 similarly enhanced activation of infiltrated MOG-specific T cells, but not of the bystander cells (Fig. 5*C*).

Enhancement of clinical disease was less pronounced for the TAP mutant in comparison to the MOG Ab r8-18C5 and the SAI mutant (Fig. 4), demonstrated by the lower T cell numbers and activation state of the T cells (Fig. 5*C*). The TAP mutant still showed slightly enhanced T cell infiltration compared to the control mAb HK3 (Fig. 5*C*), which might be due to the incompletely abolished binding to FcγRIIb and FcγRIII (Fig. 1 *E* and *F*).

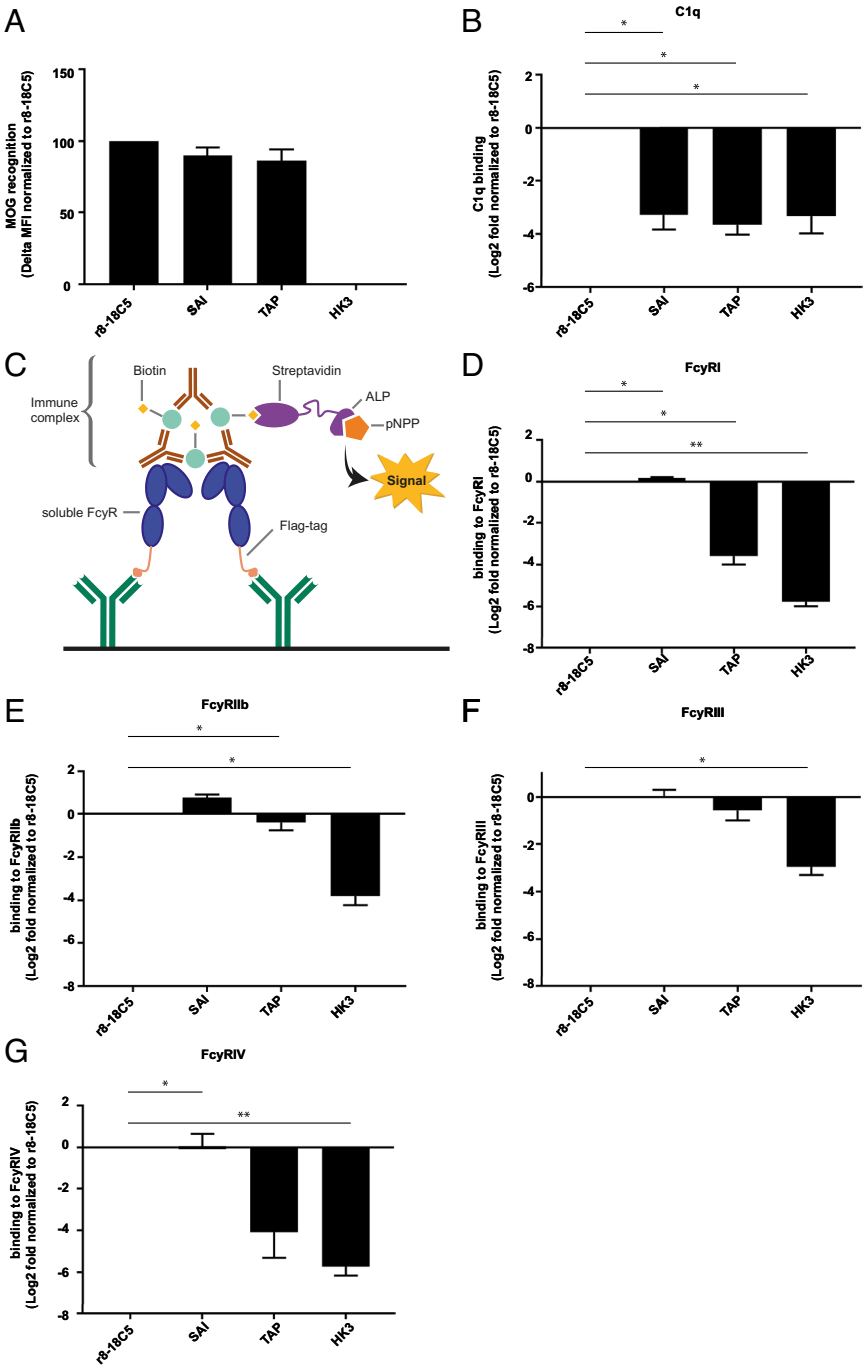

Fig. 1. Antigen recognition, C1q- and FcγR-binding of mutated MOG-specific mAbs. The MOG antibody r8-18C5 and the Fc mutant antibodies SAI and TAP show comparable binding to MOG in a cell-based flow cytometry assay (*A*). IgG binding to MOG was normalized to binding of the r8-18C5 and the assay was repeated two times for each antibody (delta MFI value). (*B*) C1q binding was analyzed with an ELISA. Specifically, ED-hMOG was coated and indicated Ab variants were added. Subsequently, C1q was added and its binding was quantified using anti-C1q Ab. Binding of the mutant Abs was normalized to the binding of the antibody r8-18C5 and the assay was repeated three times for each antibody. FcγRI, FcγRIIb, FcγRIII, and FcγRIV binding was investigated by ELISA (*C*–*G*). Anti-FLAG antibodies were coated on an ELISA plate and used to capture soluble flag-tagged FcγR (FcγRI, FcγRIIb, FcγRIII, FcγRIV) (*C*). Binding of antibody-MOG IgG immune complexes to the added soluble FcγRs was quantified (*D*-*G*). Binding of the mutant MOG-Abs SAI and TAP is normalized to the binding of the MOG antibody r8-18C5. The assay was repeated three times for each antibody. Data are shown as mean with SEM. Each mutant mAbs' affinity to C1q and FcγRs was presented as $\log_2$ fold change compared to r8-18C5 measured on the same plate and was analyzed using 2-tailed one-sample *t* test (parametric Welch's *t* test) with Benjamini–Hochberg multiple comparison correction (n = 3).

Discussion

Here, we dissect the role of complement and FcγR engagement in order to identify the main pathomechanisms of MOG-Abs. The classical effect of MOG-Abs is demyelination (33). Our study shows that about half of the demyelination mediated by MOG-Abs occurs via FcR activation and the other half is complement dependent. In previous transfer experiments with patient-derived MOG-specific IgG, we detected C9neo deposition in demyelinated areas (32). Histopathological analysis of MOGAD patients first in case reports (21, 40, 41) and then in larger patient series (19, 20) also revealed C9neo deposition in some but not all patients with MOGAD and active demyelination, suggesting that demyelination might be induced in the absence of complement-mediated cytotoxicity. Importantly, consensus is emerging that C9neo deposition is much more prominent in NMOSD than that in MOGAD (4, 16, 42). Thus, our finding of complement-independent demyelination by MOG-Abs may provide an explanation of the histological observation of active demyelination in MOGAD patients in the absence of C9neo deposition.

A monovalent binding of IgG has been reported to facilitate the formation of a hexameric platform for C1q binding (43); however, bivalently bound IgG recognizing certain target antigens may also induce complement activation (44). Our previous work has shown that MOG-Abs from patients require bivalent binding (45). The intracellular part of MOG enhances recognition of its extracellular part by MOG-Abs from patients, presumably because

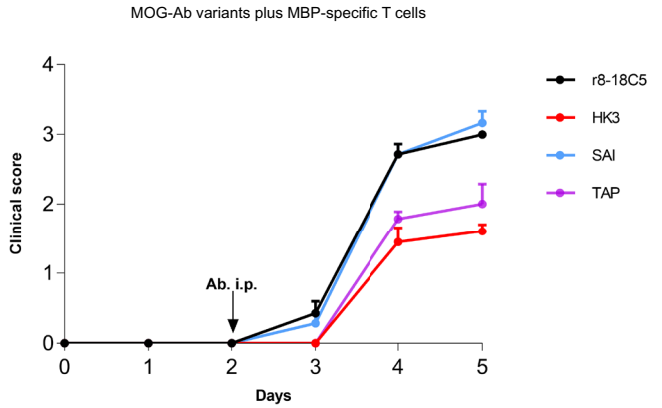

Fig. 2. Clinical EAE in the model with MBP-specific T cells and mutated MOG-Abs. Lewis rats were injected with MBP-specific T cells that strongly breach the blood–brain barrier. At day 2, the indicated nonmutated MOG-Abs, the mutated MOG-Abs (TAP, SAI), and the control Ab HK3 were injected intraperitoneally. Histology was performed at day 4 or 5. We investigated the development of the clinical disease over time. The clinical score displayed represents the mean + SEM of the following number of animals. r8-18C5 (day 4, n = 5; day 5, n = 2), SAI (day 4, n = 4; day 5, n = 3), TAP (day 4, n = 4; day 5, n = 3), HK3 (day 4, n = 4; day 5, n = 5). Day 4: r8-18C5 vs. SAI = ns; r8-18C5 vs. TAP $P \leq 0.01$; 8-18C5 vs. HK3 $P < 0.0001$; SAI vs. TAP $P \leq 0.01$; SAI vs. HK3 $P < 0.0001$; TAP vs. HK3 = ns. Day 5: r8-18C5 vs. SAI = ns; r8-18C5 vs. TAP $P \leq 0.05$; 8-18C5 vs. HK3 $P \leq 0.01$; SAI vs. TAP $P \leq 0.01$; SAI vs. HK3 $P \leq 0.001$; TAP vs. HK3 = ns.

the second hydrophobic domain of MOG induces a spacing of MOG that facilitates bivalent binding (45). Our study shows that MOG-Abs also induce demyelination independent of C1q binding and this highlights the role of FcγR activation in MOGAD.

The second pathomechanism of MOG-Abs is enhancement of the activation of cognate T cells (28, 29, 32). We show that this is independent of C1q binding but mediated via FcγR binding. This extends the previous observation that the Fc-part of MOG-Abs is essential for cognate T cell activation presumably by enhanced antigen uptake by local antigen-presenting cells (29). It is unknown where the MOG-Abs recognize their antigen when they enhance the activation of cognate T cells. Furthermore, it is unclear which cell type in the CNS is mediating this FcγR-dependent T cell activation and which types of FcRs are involved in this. In addition to enhancing activation of cognate T cells, MOG-Abs stimulate microglia via FcRs and Bruton's tyrosine kinase (BTK) engagement (46).

The demonstration that MOG-Abs are pathogenic by enhancing MOG-specific T cells calls for further work on MOG-specific T cells in MOGAD using technical advances in the recognition of rare MOG-specific T cells (47, 48).

Comparison to NMOSD and Therapeutic Implications. Currently, no therapy for MOGAD has been approved. Understanding the pathomechanisms of autoantibodies, however, can result in therapeutic success as seen in the clinically related disorder NMOSD (4, 49, 50). This disease is characterized by pathogenic auto-Abs to the astrocyte protein AQP4 (51). Complement-mediated pathogenic effects of anti-AQP4 Abs have been proposed based on pathology, transfer experiments, and detailed in vitro analysis (13–16). Based on these findings, eculizumab which targets the complement factor C5 has been tested in NMOSD patients with impressive clinical success (4, 49, 50). In MOGAD, complement protein concentration in serum was analyzed. One study reported serum complement C4 levels to be higher in 15 patients with MOGAD as compared to 16 patients with NMOSD, suggesting higher complement consumption in the latter (52). Another study profiled systemic complement activation in 109 patients with MOGAD and reported elevated levels of activated complement proteins in MOGAD compared to relapse-onset multiple sclerosis, pediatric control, and adult

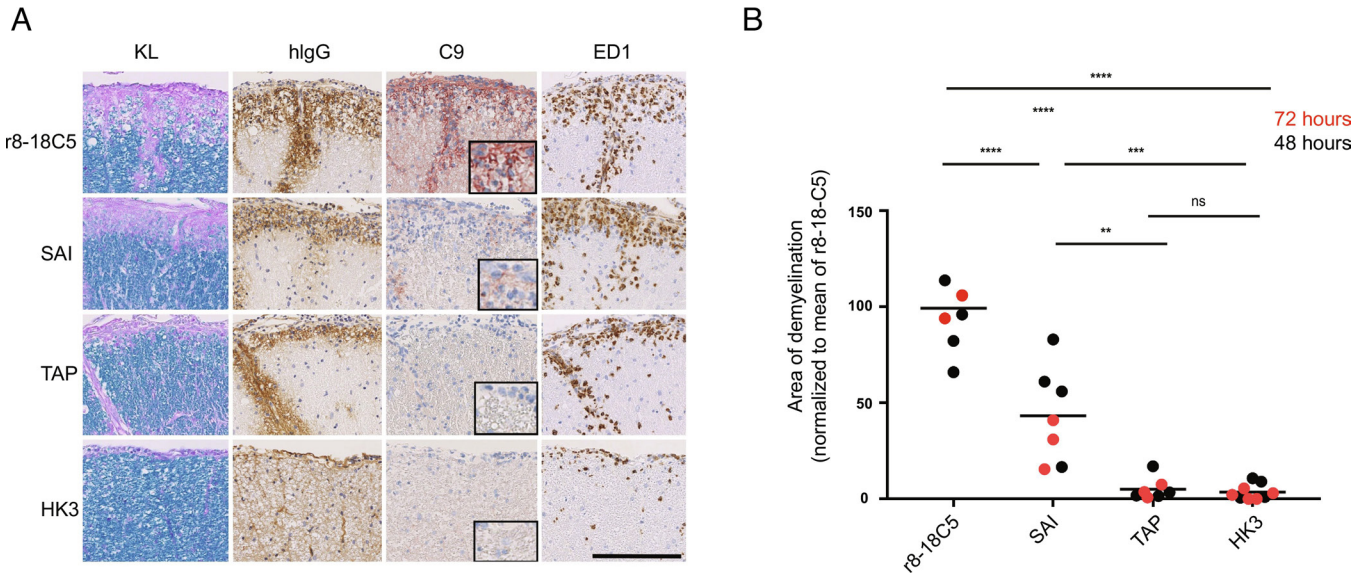

Fig. 3. Histopathology of the EAE induced by MBP-specific T cells and mutated MOG antibodies. Spinal cord sections of Lewis rats, which developed EAE subsequent to transfer of T cells specific for MBP (*A* and *B*). Animals were intraperitoneally injected 72 h prior to the analysis (day 5) with the MOG-specific antibodies r8-18C5 (positive control), SAI (abolished C1q binding with intact FcγR binding), or TAP (abolished binding to C1q and to FcγRI and FcγRIV). The antibody HK3 was used as negative control. For each experimental animal, consecutive spinal cord sections were subjected to Kluver–Barrera (KL) staining to show the presence (turquoise) or absence (light blue/pink) of myelin, or to stainings with antibodies specific for human immunoglobulin G (hIgG, brown) to reveal the presence of the antibodies in the tissue, for complement C9neo (C9neo, red) to reveal the terminal membrane attack complex as indicator for complement-dependent (cellular) cytotoxicity, and with the antibody ED1 (brown) specific for macrophages/activated microglia needed for antibody-dependent cellular cytotoxicity. Counterstaining was done with hematoxylin to reveal nuclei (blue). Bar = 100 μm. (*B*) The spinal cords were used for the quantification of demyelination of animals after 48 h of antibody injection (black dots) or 72 h (red dots) of injection. We normalized the 48-h animals (TAP, SAI, and HK3) to the mean value of demyelination (mm2) of all rats for r8-18C5 and expressed it as percentage. In the same figure, we also merged the 72-h animals which we label in red (normalized to the r8-18C5 after 72 h). One-way ANOVA with Tukey's test (four groups) was performed for comparison between groups. $P < 0.05$ was considered significant.

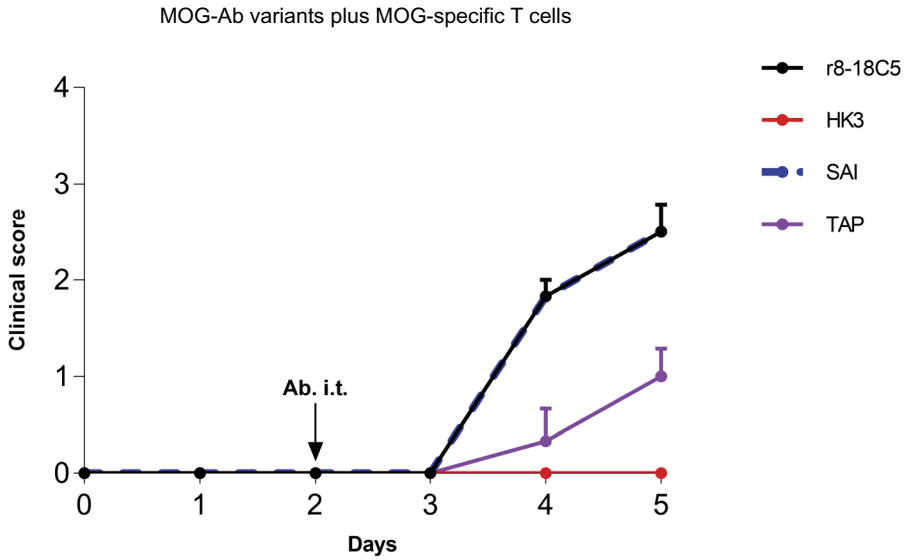

Fig. 4. Clinical EAE in the model with cognate MOG-specific T cells and mutated MOG-Abs. Lewis rats were injected with MOG-specific T cells that do not induce clinical disease on their own. At day 2, the indicated nonmutated MOG-Abs, the mutated MOG-Abs, and the control Ab HK3 were injected intraperitoneally. Histology and FACS analysis of the infiltrates were performed at day 5. Development of the clinical disease over time. The clinical score displayed represents the mean + SEM of the following number of animals. r8-18C5 (n = 3), SAI (n = 3), TAP (n = 3), HK3 (n = 3). One-way ANOVA with Tukey's test (four groups) was performed for comparison between groups. $P < 0.05$ was considered significant. Day 4: r8-18C5 vs. SAI = ns; r8-18C5 vs. TAP $P \leq 0.01$; r8-18C5 vs. HK3 $P \leq 0.001$; SAI vs. TAP $P \leq 0.01$; SAI vs. HK3 $P \leq 0.001$; TAP vs. HK3 = ns. Day 5: r18C5 vs. SAI =ns; 8-18C5 vs. TAP $P \leq 0.05$; r8-18C5 vs. HK3 ≤ 0.001(***), SAI 5 vs. TAP $P \leq 0.05$; SAI vs. HK3 $P \leq 0.001$; TAP vs. HK3 = ns.

healthy donors (53). Enhanced complement activation was, however, not associated with clinical disease activity (53). Recently, an in vitro assay showed more efficient complement activation by anti-AQP4 autoantibodies from NMOSD patients compared to anti-MOG antibodies from MOGAD patients (26). These in vitro data with patient Abs and our in vivo data

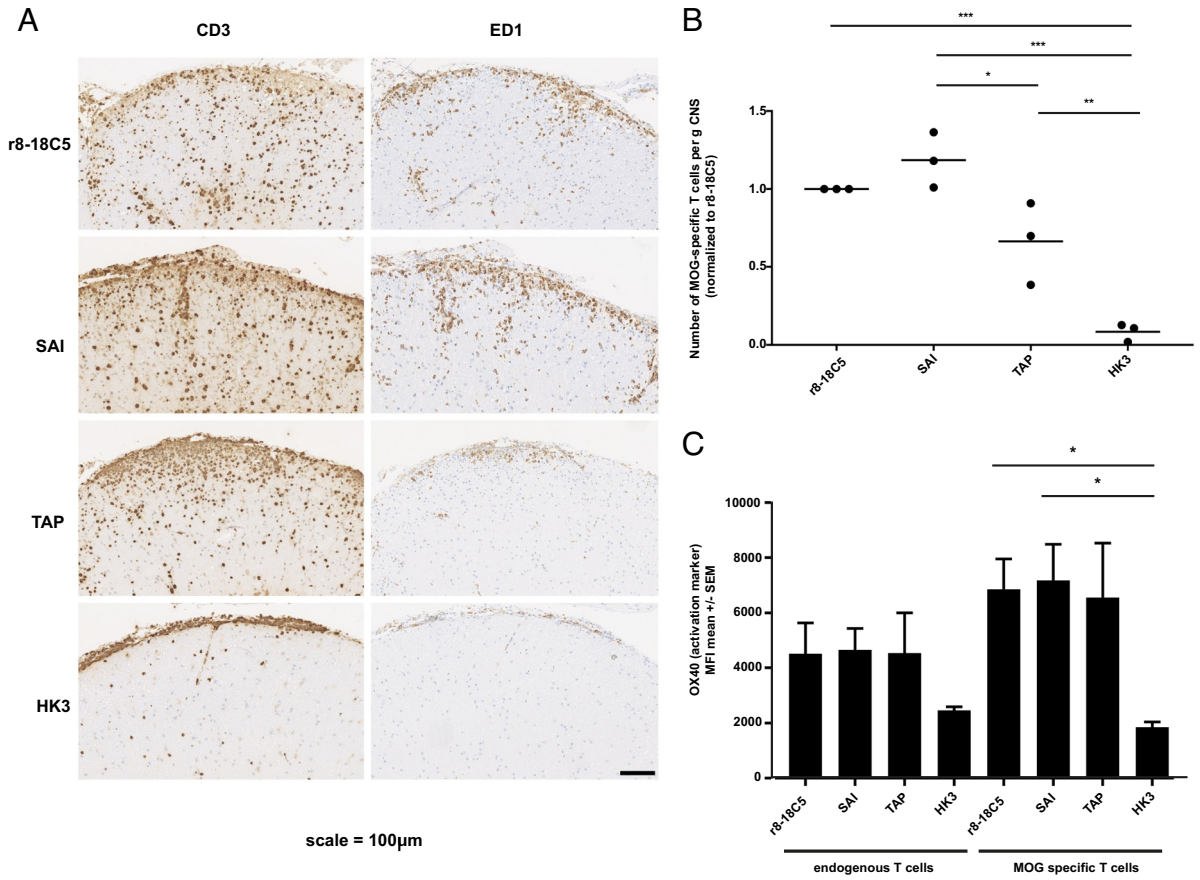

Fig. 5. Pathology of the EAE induced by MOG-specific T cells and mutated MOG antibodies. Lewis rats received MOG-specific T cells 2 d before the MOG-specific antibodies r8-18-C5 (positive control), SAI (abolished C1q binding and intact FcγR binding), TAP (abolished C1q binding and abolished binding to FcγRI and FcγRIV), or the control Ab HK3 were injected. After 72 h, about half of the spinal cords were fixed with PFA, embedded, and analyzed for histopathology (*A* and *B*), while the other half of the spinal cords were processed for FACS analysis (*C*). (*A* and *B*) For each experimental animal, consecutive spinal cord sections were stained with anti-CD3 antibodies to visualize T cells (brown) and the ED1 antibody to show macrophages/activated microglia (brown). Counterstaining was done with hematoxylin to reveal nuclei (blue). Bar = 100 µm. (*C*) The same spinal cords were used for the quantification of T cells via flow cytometry and their activation status reflected by OX40 expression was determined. MOG-specific T cells were separated from endogenous bystander T cells by their fluorescence properties. The number of MOG-specific T cells is displayed in relation to the amount observed after injection of the r8-18C5 (set as 1). (*C*) The activation status of endogenous bystander T cells and injected MOG-specific T cells in the CNS inflammatory lesions was determined by staining for the activation marker OX40. One-way ANOVA with Tukey's test (four groups) was performed for comparison between groups. $P < 0.05$ was considered significant.

with mutated mAbs suggest that targeting complement in MOGAD might be less effective than that in NMOSD.

Limitations. Although we identify the pathomechanisms of MOG-Abs that are mediated by FcγRs, our in vivo study does not allow us to dissect which FcγR is mediating the demyelination and enhancement of cognate T cell activation. To address this, a transfer model should be established allowing deletion or antibody-mediated blocking of individual FcγRs (54, 55). Our mutated Ab-variant reveals pathology independent of C1q binding, but this does not exclude a role of the alternative pathway of complement activation in MOG Ab-mediated pathology. Nevertheless, our observation that the lack of C1q binding is associated with a lack of C9neo deposition, which is also an end product of the alternative complement pathway, argues against an important role of the alternative pathway. As highly pathogenic mAbs from patients with MOGAD are not available, we used the mAb r8-18C5. Since our previous transfer experiments with polyclonal human MOG-Abs and this humanized r8-18C5 revealed that they were similarly pathogenic in both animal models (32), we believe that the analysis of the mutated humanized r8-18C5 provides useful information to assess the mechanistic details of human MOG-Abs. We used a humanized version of the classical MOG mAb r8-18C5 with a human IgG1, since human MOG-Abs are mainly IgG1 subtype (36). Further work will have to establish MOG-specific mAbs from patients, who show heterogeneity in details of antigen recognition (45, 56–58). It is also possible that CDC plays a more prominent role in some MOGAD patients than others.

Taken together, we could dissect FcγR and complement-mediated pathomechanisms of MOG-Abs. This has important implications for harnessing MOG-IgG-mediated autoimmunity in animal models. Importantly, this study has direct implications for the development of therapeutic strategies in patients with MOGAD. We suggest that targeting complement will be less efficient in MOGAD than in NMOSD and rather propose to use next-generation FcγR blocking reagents (59, 60) in patients with MOGAD.

Materials and Methods

Generation of Fc Mutant Antibodies. Thirteen different Fc mutant antibodies of the humanized recombinant mouse antibody r8-18C5 were generated using site-directed mutagenesis (SDM). Specifically, point mutations were introduced into the heavy chain of the IgG antibody. Mutation nomenclature is according to Kabat EU index (61). For each SDM, a reaction solution with 10 ng/μL DNA template, 200 μM dNTP, 1X Phusion® HF Buffer, 3% DMSO, 0.2 U/μL Phusion® HF DNA Polymerase, and 0.5 μM of each primer was prepared on ice and supplemented with nuclease-free water to 50 μL. Following PCR, maternal DNA was digested using 0.4 U/mL Dpn I restriction enzyme and incubated at 37 °C for 1 h. Subsequently, DH5α-competent cells were transformed by heat shock. DNA was isolated and sequences were confirmed by the sequencing service of the Faculty of Biology (LMU Bio Center, Martinsried). Ig heavy and light chain vector pairs were transiently transfected into HEK EBNA cells using Polyethylenimine (Polysciences) and the cells were cultured in Freestyle Medium 293 supplemented with 1% Pluronic F68 (Gibco) and 25 μg/mL Geneticin (Gibco). Supernatants were harvested after 4 d of culture. Antibody purification was performed by immobilized metal affinity chromatography as previously described (32). As a quality control, all antibodies were analyzed for integrity using nonreducing SDS page. Antibody concentrations were quantified with nanodrop and human IgG ELISA development kit (Mabtech, Nacka Strand, Sweden) as previously described (62).

Recognition of Cell-Based MOG. The MOG recognition was determined as previously described (32, 45). Briefly, cells were transfected with full-length MOG fused to EGFP or EGFP alone. MOG reactivity of the different variants of r8-18C5 was evaluated by determining the delta MFI (MFI of MOG-EGFP transfected cells–MFI of EGFP-transfected cells). The MOG-EGFP transfected cells or EGFP control cells were incubated with the mAb at a concentration of 0.5 μg/mL.

C1q ELISA. A 96-well MaxiSorp plate was coated with the extracellular part of MOG (called ED-hMOG) which is correctly folded as seen by circular dichroism (32). Then, 100 μL of 1 μg/mL ED-hMOG (capture antigen) diluted in PBS was added and incubated over night at 4 °C on a shaker. The next day, the plate was washed three times with PBS (200 μL/well), followed by a blocking step (200 μL/well, 3% BSA/PBS-T) for 2 h at RT on a shaker. After blocking, the plate was washed five times with PBS-T, and 100 μL/well of samples diluted in 0.5% BSA/PBS-T was added and incubated over night at 4 °C on a shaker. On the following day, the plate was washed five times with PBS-T, and 100 μL/well of 5 μg/mL human C1q (Sigma Aldrich) molecule was added and incubated for one hour at RT on a shaker. Afterward, the plate was washed again five times with PBS-T. For detection, 100 μL/well of an anti-C1q-HRP antibody diluted 1:200 in 0.5% BSA/PBS-T was added, followed by washing five times with PBS-T. As a substrate, 100 μL/well of 3,3′,5,5′-Tetramethylbenzidine was added and incubated for 6 min. The enzymatic reaction was stopped by adding 50 μL/well of H_2SO_4 and then the optical density was measured at 450 nm and 540 nm (background) with the Victor2 plate reader (PerkinElmer). Fold change was calculated for each mutant mAb's averaged optical density in comparison to the averaged optical density of the strong C1q binder r8-18C5, which was measured on the same plate. Data are presented as $\log_2$ (fold change).

IgG-IC-FcγR-ELISA. Binding of MOG-specific IgG to FcγR was assessed for IgG immune complexes (IgG-IC) by ELISA. Briefly, a 96-well MaxiSorp plate was coated with 100 μL/well of 5 μg/mL anti-FLAG Ab M2 (Merck) diluted in carbonate–bicarbonate coating buffer and incubated overnight at 4 °C on a shaker. The next day, the plate was washed three times with 200 μL/well of PBS, followed by a blocking step with 200 μL/well of 3% BSA/PBS-T for 2 h at RT on a shaker. After blocking, the plate was washed three times with PBS-T and the soluble flag-tagged murine FcγRI, FcγRIIB, FcγRIII, and FcγRIV [generated as previously described (63)] was added and incubated over night at 4 °C on a shaker. On the following day, immune complexes were formed by mixing 200 ng/well of anti-MOG antibodies and isotype control HK3 (32) with 100 ng/well of biotinylated ED-hMOG (32, 45) and incubated for three hours in a multirotator at 30 rpm. The plate was washed five times with PBS-T, 50 μL/well of immune complexes was added, and incubated for two hours at RT on a shaker. Afterward, the plate was washed again five times with PBS-T. For detection, 100 μL/well of streptavidin-ALP diluted 1:1,000 in 0.5% BSA/PBS-T was added, followed by washing five times with PBS-T. As a substrate, 100 μL/well of pNPP was added and incubated up to 300 min. The optical density was measured at 450 nm and 650 nm (background) with the Multiskan FC (Thermo Fisher Scientific).

T Cell-Mediated Transfer of EAE. Antigen-specific T cells were generated as described (32, 35). Briefly, Lewis rats were immunized with MBP (from guinea pig brain) or recombinant rat MOG (amino acid 1 to 125) emulsified in complete Freund adjuvant. Restimulated MOG-specific T cells [15×10^6, genetically labeled with a fluorescence protein (64)] or MBP-specific T cells (1×10^6) were intravenously injected to induce EAE, and standard scoring of EAE was applied. The antibodies (r8-18C5, HK3, SAI, TAP) were injected two days after T cell injection either intraperitoneally (1 mg in 1 mL IgG for MBP-EAE) or intrathecally into the cisterna magna (100 μg in 100 μL IgG for the MOG-EAE) (32, 35).

For intrathecal injection, the animals were anesthetized by fentanyl/midazolam/medetomidin. The animals were killed 48 (MBP-T cell EAE) or 72 h (MBP-T cell EAE and MOG-T cell EAE) after antibody injection. For histology, the animals were perfused with PBS and 4% PFA in PBS after euthanasia; the spinal cord and brain were then postfixed with 4% PFA in PBS at 4 °C for 24 h and stored in PBS at 4 °C. All animal procedures were approved by the Government of Oberbayern and we followed the ARRIVE guidelines for animal studies.

Immunohistochemistry. Sections were immersed in xylol for 30 min, transferred to 96% ethanol, and incubated in 0.2% hydrogen peroxide for 30 min to block endogenous peroxidase. Then, the sections were rehydrated through a descending ethanol series (96, 70, 50%) and rinsed in distilled water. Prior to the incubation with specific antibodies detailed below, the sections were subjected to antigen retrieval by heating them for 30 min (in the case of ED1 antibodies) or 60 min (in the case of anti-CD3 antibodies) in 10 mM EDTA pH 8.5 in a conventional household steamer, or were incubated for 15 min at 37 °C in 0.03%

protease-type XXIV (Sigma-Aldrich, Vienna, Austria; in the case of anti-C9neo antibodies or biotinylated-anti-human IgG antibodies). Subsequently, the sections were rinsed in 0.1 M PBS or Tris-buffered saline for 60 min and exposed to 10% fetal calf serum in 1 x Wash Buffer (Dako) in PBS for 20 min at room temperature to reduce nonspecific background. Then, immunohistochemical stainings were done using the following antibodies: As primary antibodies, rabbit anti-rat C9neo (1:2,000) (65), monoclonal rabbit anti-human CD3 (cross-reactive to rat CD3; 1:2,000; Thermo Scientific, Vienna, Austria), monoclonal mouse anti-rat ED1 (1:10,000; Thermo Scientific, Vienna, Austria), and biotinylated anti-human IgG (1:1,000, Szabo Scandic, Vienna, Austria) were added, and the sections were incubated overnight at 4 °C in a moist chamber. After several washes, sections which had been incubated with rabbit anti-human CD3, rabbit anti-rat C9neo, or mouse anti-rat ED1 were further reacted with biotinylated donkey anti-rabbit (1:1,000 to 1:2,000, Jackson ImmunoResearch) or biotinylated sheep anti-mouse antibodies (1:500, Jackson ImmunoResearch) for 1 h at room temperature. All reactions were completed with AEC system (for C9neo) or by exposure to the avidin-peroxidase complex (1:200, Amersham GE Healthcare) and subsequent visualization with 3,3′ diaminobenzidine-tetra-hydrochloride (DAB, Sigma) containing 0.01% hydrogen peroxide (all other antibodies). Finally, the tissue sections were counterstained with hematoxylin and mounted in geltol (sections developed with the AEC system), or dehydrated and mounted in Eukitt© (Merck, Darmstadt, Germany) (all other sections).

Kluver–Barrera Staining. Sections were immersed in xylol for 30 min, transferred to 96% ethanol, and incubated overnight with 0.1% Luxol Fast Blue in 96% ethanol at 56 to 60 °C. Then, the sections were cooled to room temperature, washed in 96% ethanol, rinsed in distilled water, and incubated for 5 min with 0.1% lithium carbonate in water. Subsequently, the sections were washed with 70% ethanol until the background staining was removed. The sections were then rinsed with distilled water, immersed for 10 min in 0.8% periodic acid in water, rinsed with distilled water, and incubated for 20 min in Schiff´s reagent (Roth, Karlsruhe, Germany). After 3× washing for 2 min in sulfite wash solution (0.37% HCl with 2.5% potassium metabisulfite in water), the sections were washed for 5 to 10 min in tap water, dehydrated, and mounted in Eukitt©. With this staining procedure, myelin sheaths of the CNS appear turquoise, and CNS gray matter pink.

Lesion Evaluation. After Kluver–Barrera staining, all tissue sections were scanned and evaluated with the viewing software NDP.view2 (Hamamatsu Photonics K.K., Japan) for quantification of myelin loss in EAE animals, 48 h after the injection of the antibodies. For each experimental animal, the 2 lumbar/sacral tissue sections affected most by myelin loss were selected to determine both the complete area of the spinal cord section and the complete area with demyelination seen in this section, and to calculate the size of the demyelinated area per mm^2 of the spinal cord section. We then normalized the different experimental groups to the mean value of demyelination/mm^2 of the positive control group (= the group of animals receiving r8-18C5).

Quantification of MOG-Specific T Cells in the Inflamed CNS. After euthanasia, spinal cord parenchyma was prepared and the weight of the organ was measured. Then, the organ was homogenized by pasting metal sieve and resuspending in defined amount of DMEM supplemented with 25mM HEPES. Then, 1×10^4 fluorescent-labeled beads (Becton Dickinson) (identified through labeling with PE) were added into 100 µL cell suspension. The numbers of beads and MOG-specific T cells [identified through labeling with GFP (64)] were measured by FACS VERSE (Becton Dickinson). The obtained results were analyzed by FlowJo software.

Statistics. Statistical analyses were performed using GraphPad Prism 7 (GraphPad Software Inc., La Jolla, CA, USA). Individual statistical tests are stated in the figure legends. $P < 0.05$ was considered statistically significant (*), $P \leq 0.01$ (**), $P \leq 0.001$(***), $P < 0.0001$(****).

Data, Materials, and Software Availability. All study data are included in the article and/or *SI Appendix*.

ACKNOWLEDGMENTS. We thank Prof. Dr. Hartmut Wekerle and Prof. Dr. Reinhard Hohlfeld, Dr. Anneli Peters, and Dr. Eduardo Beltrán for comments on the manuscript. We would like to thank Dr. Tobias Straub for statistical advice, the Core Facility Animal Models for animal husbandry and Ulrike Köck for excellent technical assistance. This work was supported by the Deutsche Forschungsgemeinschaft (DFG; German research foundation; SFB TR128) (to E.M., N.K., and J.D.L.) and by DFG (CRC1526-A07, TRR305-B02, NI711/9-1, NI711/11-1 to F.N.), the Verein zur Therapieforschung für MS Kranke (to E.M.), and the Else Kröner-Fresenius-Stiftung (to S.M.).

Author affiliations: [a]Institute of Clinical Neuroimmunology, Biomedical Center and University Hospital, Ludwig-Maximilians-Universität München, 82152 Planegg-Martinsried, Germany; [b]Graduate School of Systemic Neuroscience, Ludwig-Maximilians-Universität München, 82152 Planegg-Martinsried, Germany; [c]Chair of Genetics, Department of Biology, Friedrich Alexander University of Erlangen-Nürnberg, 91058 Erlangen, Germany; [d]Department of Neurology with Institute of Translational Neurology, University Hospital Münster, 48149 Münster, Germany; [e]Medical Immunology Campus Erlangen, Friedrich-Alexander University Erlangen-Nürnberg, Erlangen 91058, Germany; and [f]Department of Neuroimmunology, Center for Brain Research, Medical University of Vienna, 1090 Vienna, Austria

Author contributions: S.M., S.H., H.K.W., S.B., S.W., H.R., I.M.F., R.G., C.D., O.C., J.D.L., A.L., F.N., M.B., N.K., and E.M. designed research; S.M., S.H., H.K.W., S.B., S.W., C.R., H.R., I.M.F., R.G., C.D., O.C., J.D.L., A.L., F.N., M.B., and N.K. performed research; S.M., C.R., A.L., F.N., M.B., N.K., and E.M. contributed new reagents/analytic tools; S.M., S.H., H.K.W., S.B., S.W., C.R., H.R., I.M.F., R.G., C.D., O.C., J.D.L., A.L., F.N., M.B., N.K., and E.M. analyzed data; and S.M., S.H., H.K.W., S.B., S.W., C.R., H.R., I.M.F., R.G., C.D., O.C., J.D.L., A.L., F.N., M.B., N.K., and E.M. wrote the paper.

1. J. Dalmau, F. Graus, Antibody-mediated encephalitis. *N. Engl. J. Med.* **378**, 840–851 (2018), 10.1056/NEJMra1708712.
2. H. Prüss, Autoantibodies in neurological disease. *Nat. Rev. Immunol.* **21**, 798–813 (2021), 10.1038/s41577-021-00543-w.
3. R. J. Ludwig *et al.*, Mechanisms of autoantibody-induced pathology. *Front. Immunol.* **8**, 603 (2017), 10.3389/fimmu.2017.00603.
4. S. Mader, T. Kumpfel, E. Meinl, Novel insights into pathophysiology and therapeutic possibilities reveal further differences between AQP4-IgG- and MOG-IgG-associated diseases. *Curr. Opin. Neurol.* **33**, 362–371 (2020), 10.1097/wco.0000000000000813.
5. D. S. W. Lee, O. L. Rojas, J. L. Gommerman, B cell depletion therapies in autoimmune disease: Advances and mechanistic insights. *Nat. Rev. Drug Discov.* **20**, 179–199 (2021), 10.1038/s41573-020-00092-2.
6. S. J. Pittock, A. Zekeridou, B. G. Weinshenker, Hope for patients with neuromyelitis optica spectrum disorders–from mechanisms to trials. *Nat. Rev. Neurol.* **17**, 759–773 (2021), 10.1038/s41582-021-00568-8.
7. M. Levy, K. Fujihara, J. Palace, New therapies for neuromyelitis optica spectrum disorder. *Lancet Neurol.* **20**, 60–67 (2021), 10.1016/S1474-4422(20)30392-6.
8. J. L. Bennett *et al.*, Optic neuritis and autoimmune optic neuropathies: Advances in diagnosis and treatment. *Lancet Neurol.* **22**, 89–100 (2023), 10.1016/S1474-4422(22)00187-9.
9. M. Reindl, P. Waters, Myelin oligodendrocyte glycoprotein antibodies in neurological disease. *Nat. Rev. Neurol.* **15**, 89–102 (2019), 10.1038/s41582-018-0112-x.
10. R. Marignier *et al.*, Myelin-oligodendrocyte glycoprotein antibody-associated disease. *Lancet Neurol.* **20**, 762–772 (2021), 10.1016/s1474-4422(21)00218-0.
11. E. Melamed *et al.*, Update on biomarkers in neuromyelitis optica. *Neurol. Neuroimmunol. NeuroInflamm.* **2**, e134 (2015), 10.1212/nxi.0000000000000134.
12. M. Jurynczyk *et al.*, Clinical presentation and prognosis in MOG-antibody disease: A UK study. *Brain.* **140**, 3128–3138 (2017), 10.1093/brain/awx276.
13. P. W. Phuan, J. Ratelade, A. Rossi, L. Tradtrantip, A. S. Verkman, Complement-dependent cytotoxicity in neuromyelitis optica requires aquaporin-4 protein assembly in orthogonal arrays. *J. Biol. Chem.* **287**, 13829–13839 (2012), 10.1074/jbc.M112.344325.
14. J. Soltys *et al.*, Membrane assembly of aquaporin-4 autoantibodies regulates classical complement activation in neuromyelitis optica. *J. Clin. Investig.* **129**, 2000–2013 (2019), 10.1172/jci122942.
15. M. Bradl *et al.*, Neuromyelitis optica: Pathogenicity of patient immunoglobulin in vivo. *Ann. Neurol.* **66**, 630–643 (2009).
16. Y. Takai *et al.*, Staging of astrocytopathy and complement activation in neuromyelitis optica spectrum disorders. *Brain.* **144**, 2401–2415 (2021), 10.1093/brain/awab102.
17. J. Ratelade *et al.*, Involvement of antibody-dependent cell-mediated cytotoxicity in inflammatory demyelination in a mouse model of neuromyelitis optica. *Acta Neuropathol.* **126**, 699–709 (2013), 10.1007/s00401-013-1172-z.
18. D. M. Wingerchuk *et al.*, Long-term safety and efficacy of eculizumab in aquaporin-4 IgG-positive NMOSD. *Ann. Neurol.* **89**, 1088–1098 (2021), 10.1002/ana.26049.
19. R. Hoftberger *et al.*, The pathology of central nervous system inflammatory demyelinating disease accompanying myelin oligodendrocyte glycoprotein autoantibody. *Acta Neuropathol.* **139**, 875–892 (2020), 10.1007/s00401-020-02132-y.
20. Y. Takai *et al.*, Myelin oligodendrocyte glycoprotein antibody-associated disease: An immunopathological study. *Brain* **143**, 1431–1446 (2020), 10.1093/brain/awaa102.
21. M. Spadaro *et al.*, Histopathology and clinical course of MOG-antibody associated encephalomyelitis. *Ann. Clin. Transl. Neurol.* **2**, 295–301 (2015).
22. R. C. Dale *et al.*, Antibodies to MOG have a demyelination phenotype and affect oligodendrocyte cytoskeleton. *Neurol. Neuroimmunol. Neuroinflamm.* **1**, e12 (2014), 10.1212/nxi.0000000000000012.
23. F. Brilot *et al.*, Antibodies to native myelin oligodendrocyte glycoprotein in children with inflammatory demyelinating central nervous system disease. *Ann. Neurol.* **66**, 833–842 (2009).

24. S. Mader *et al.*, Complement activating antibodies to myelin oligodendrocyte glycoprotein in neuromyelitis optica and related disorders. *J. Neuroinflamm.* **8**, 184 (2011), 10.1186/1742-2094-8-184.
25. P. Peschl *et al.*, Human antibodies against the myelin oligodendrocyte glycoprotein can cause complement-dependent demyelination. *J. Neuroinflamm.* **14**, 208 (2017), 10.1186/s12974-017-0984-5.
26. M. Lerch *et al.*, More efficient complement activation by anti-aquaporin-4 compared with anti-myelin oligodendrocyte glycoprotein antibodies. *Neurol. Neuroimmunol. Neuroinflamm.* **10**, e200059 (2023), 10.1212/NXI.0000000000200059.
27. S. Saadoun *et al.*, Neuromyelitis optica MOG-IgG causes reversible lesions in mouse brain. *Acta Neuropathol. Commun.* **2**, 35 (2014), 10.1186/2051-5960-2-35.
28. A. C. Flach *et al.*, Autoantibody-boosted T-cell reactivation in the target organ triggers manifestation of autoimmune CNS disease. *Proc. Natl. Acad. Sci. U.S.A.* **113**, 3323–3328 (2016), 10.1073/pnas.1519608113.
29. S. Kinzel *et al.*, Myelin-reactive antibodies initiate T cell-mediated CNS autoimmune disease by opsonization of endogenous antigen. *Acta Neuropathol.* **132**, 43–58 (2016), 10.1007/s00401-016-1559-8.
30. P. Khare *et al.*, Myelin oligodendrocyte glycoprotein-specific antibodies from multiple sclerosis patients exacerbate disease in a humanized mouse model. *J. Autoimmun.* **86**, 104–115 (2018), 10.1016/j.jaut.2017.09.002.
31. H. J. Schluesener, R. A. Sobel, C. Linington, H. L. Weiner, A monoclonal antibody against a myelin oligodendrocyte glycoprotein induces relapses and demyelination in central nervous system autoimmune disease. *J. Immunol.* **139**, 4016–4021 (1987).
32. M. Spadaro *et al.*, Pathogenicity of human antibodies against myelin oligodendrocyte glycoprotein. *Ann Neurol.* **84**, 315–328 (2018), 10.1002/ana.25291.
33. C. Linington, M. Bradl, H. Lassmann, C. Brunner, K. Vass, Augmentation of demyelination in rat acute allergic encephalomyelitis by circulating mouse monoclonal antibodies directed against a myelin/oligodendrocyte glycoprotein. *Am J. Pathol.* **130**, 443–454 (1988).
34. T. Derfuss *et al.*, Contactin-2/TAG-1-directed autoimmunity is identified in multiple sclerosis patients and mediates gray matter pathology in animals. *Proc. Natl. Acad. Sci. U.S.A.* **106**, 8302–8307 (2009).
35. R. Gerhards *et al.*, Oligodendrocyte myelin glycoprotein as a novel target for pathogenic autoimmunity in the CNS. *Acta Neuropathol. Commun.* **8**, 207 (2020), 10.1186/s40478-020-01086-2.
36. P. Waters *et al.*, MOG cell-based assay detects non-MS patients with inflammatory neurologic disease. *Neurol. Neuroimmunol. Neuroinflamm.* **2**, e89 (2015), 10.1212/nxi.0000000000000089.
37. M. B. Overdijk *et al.*, Crosstalk between human IgG isotypes and murine effector cells. *J. Immunol.* **189**, 3430–3438 (2012), 10.4049/jimmunol.1200356.
38. J. V. Ravetch, F. Nimmerjahn, "Fc receptors and their role in immune regulation and inflammation 6th Edition" in *Fundamental Immunology*, W. E. Paul, Ed. (Lippincott Williams & Wilkins, 2008) pp. 684–705.
39. G. Dekkers *et al.*, Affinity of human IgG subclasses to mouse Fc gamma receptors. *MAbs* **9**, 767–773 (2017), 10.1080/19420862.2017.1323159.
40. S. Jarius *et al.*, Screening for MOG-IgG and 27 other anti-glial and anti-neuronal autoantibodies in 'pattern II multiple sclerosis' and brain biopsy findings in a MOG-IgG-positive case. *Mult. Scler.* **22**, 1541–1549 (2016), 10.1177/1352458515622986.
41. F. Di Pauli *et al.*, Fulminant demyelinating encephalomyelitis: Insights from antibody studies and neuropathology. *Neurol. Neuroimmunol. Neuroinflamm.* **2**, e175 (2015), 10.1212/nxi.0000000000000175.
42. M. S. Weber, T. Derfuss, I. Metz, W. Bruck, Defining distinct features of anti-MOG antibody associated central nervous system demyelination. *Ther. Adv. Neurol. Disord.* **11**, 1756286418762083 (2018), 10.1177/1756286418762083.
43. C. A. Diebolder *et al.*, Complement is activated by IgG hexamers assembled at the cell surface. *Science* **343**, 1260–1263 (2014), 10.1126/science.1248943.
44. S. Bondza *et al.*, Complement-dependent activity of CD20-specific IgG correlates with bivalent antigen binding and C1q binding strength. *Front. Immunol.* **11**, 609941 (2020), 10.3389/fimmu.2020.609941.
45. C. Macrini *et al.*, Features of MOG required for recognition by patients with MOG antibody-associated disorders. *Brain* **144**, 2375–2389 (2021), 10.1093/brain/awab105.
46. K. Pellerin *et al.*, MOG autoantibodies trigger a tightly-controlled FcR and BTK-driven microglia proliferative response. *Brain* **144**, 2361–2374 (2021), 10.1093/brain/awab231.
47. J. J. Sabatino Jr., *et al.*, Anti-CD20 therapy depletes activated myelin-specific CD8(+) T cells in multiple sclerosis. *Proc. Natl. Acad. Sci. U.S.A.* **116**, 25800–25807 (2019), 10.1073/pnas.1915309116.
48. M. Bronge *et al.*, Myelin oligodendrocyte glycoprotein revisited-sensitive detection of MOG-specific T-cells in multiple sclerosis. *J. Autoimmun.* **102**, 38–49 (2019), 10.1016/j.jaut.2019.04.013.
49. N. Asavapanumas, L. Tradtrantip, A. S. Verkman, Targeting the complement system in neuromyelitis optica spectrum disorder. *Expert Opin. Biol. Ther.* **21**, 1073–1086 (2021), 10.1080/14712598.2021.1884223.
50. P. Stathopoulos, M. C. Dalakas, The role of complement and complement therapeutics in neuromyelitis optica spectrum disorders. *Expert Rev. Clin. Immunol.* **18**, 933–945 (2022), 10.1080/1744666x.2022.2105205.
51. V. A. Lennon, T. J. Kryzer, S. J. Pittock, A. S. Verkman, S. R. Hinson, IgG marker of optic-spinal multiple sclerosis binds to the aquaporin-4 water channel. Research support, Non-U.S. Gov't. *J. Exp. Med.* **202**, 473–477 (2005), 10.1084/jem.20050304.
52. F. Pache *et al.*, C3 and C4 complement levels in AQP4-IgG-positive NMOSD and in MOGAD. *J. Neuroimmunol.* **360**, 577699 (2021), 10.1016/j.jneuroim.2021.577699.
53. C. W. Keller *et al.*, Complement activation is a prominent feature of MOGAD. *Ann. Neurol.* **90**, 976–982 (2021), 10.1002/ana.26226.
54. S. Gordan *et al.*, The immunological organ environment dictates the molecular and cellular pathways of cytotoxic antibody activity. *Cell Rep.* **29**, 3033–3046.e4 (2019), 10.1016/j.celrep.2019.10.111.
55. B. Lehmann *et al.*, Tumor location determines tissue-specific recruitment of tumor-associated macrophages and antibody-dependent immunotherapy response. *Sci. Immunol.* **2**, eaah6413 (2017), 10.1126/sciimmunol.aah6413.
56. M. C. Mayer *et al.*, Distinction and temporal stability of conformational epitopes on myelin oligodendrocyte glycoprotein recognized by patients with different inflammatory central nervous system diseases. *J. Immunol.* **191**, 3594–3604 (2013), 10.4049/jimmunol.1301296.
57. F. Tea *et al.*, Characterization of the human myelin oligodendrocyte glycoprotein antibody response in demyelination. *Acta Neuropathol. Commun.* **7**, 145 (2019), 10.1186/s40478-019-0786-3.
58. K. Schanda *et al.*, Differential binding of autoantibodies to MOG isoforms in inflammatory demyelinating diseases. *Neurol. Neuroimmunol. Neuroinflamm.* **8**, e1027 (2021), 10.1212/nxi.0000000000001027.
59. A. W. Zuercher, R. Spirig, A. Baz Morelli, T. Rowe, F. Käsermann, Next-generation Fc receptor-targeting biologics for autoimmune diseases. *Autoimmun. Rev.* **18**, 102366 (2019), 10.1016/j.autrev.2019.102366.
60. T. Ruck, F. Nimmerjahn, H. Wiendl, J. D. Lünemann, Next-generation antibody-based therapies in neurology. *Brain* **145**, 1229–1241 (2022), 10.1093/brain/awab465.
61. E. A. Kabat, T. T. Wu, H. Bilofsky, *Sequences of Immunoglobulin Chains: Tabulation Analysis of Amino Acid Sequences of Precursors, V-regions, C-regions, J-Chain BP-Microglobulins* (Department of Health, Education, Welfare, Public Health Service, National Institutes of Health, 1979).
62. S. Winklmeier *et al.*, Identification of circulating MOG-specific B cells in patients with MOG antibodies. *Neurol. Neuroimmunol. Neuroinflamm.* **6**, 625 (2019), 10.1212/nxi.0000000000000625.
63. F. Nimmerjahn, J. V. Ravetch, Analyzing antibody-Fc-receptor interactions. *Methods Mol. Biol.* **415**, 151–162 (2008), 10.1007/978-1-59745-570-1_9.
64. A. Flügel, M. Willem, T. Berkowicz, H. Wekerle, Gene transfer into CD4+ T lymphocytes: Green fluorescent protein-engineered, encephalitogenic T cells illuminate brain autoimmune responses. *Nat. Med.* **5**, 843–847 (1999), 10.1038/10567.
65. S. J. Piddlesden, H. Lassmann, S. J. Zimprich, B. P. Morgan, C. Linington, The demyelinating potential of antibodies to myelin oligodendrocyte glycoprotein is related to their ability to fix complement. *Am. J. Pathol.* **143**, 555–564 (1993).